Prevention of MKK6-Dependent Activation by Binding to p38α MAP Kinase[‡]

Jane E. Sullivan,[§] Geoffrey A. Holdgate,[§] Douglas Campbell,[||] David Timms,[⊥] Stefan Gerhardt,[#] Jason Breed,[#] Alexander L. Breeze,[#] Alun Bermingham,[§] Richard A. Pauptit,[#] Richard A. Norman,[#] Kevin J. Embrey,[#] Jon Read,[#] Wendy S. VanScyoc,[§] and Walter H. J. Ward*,[§]

Molecular Enzymology, Respiratory and Inflammation Research, Computational Chemistry, and Structural Biology, AstraZeneca, Mereside, Alderley Park, Macclesfield, Cheshire SK10 4TG, U.K.

Received August 26, 2005; Revised Manuscript Received October 21, 2005

ABSTRACT: Inhibition of p38α MAP kinase is a potential approach for the treatment of inflammatory disorders. MKK6-dependent phosphorylation on the activation loop of p38α increases its catalytic activity and affinity for ATP. An inhibitor, BIRB796, binds at a site used by the purine moiety of ATP and extends into a "selectivity pocket", which is not used by ATP. It displaces the Asp168-Phe169-Gly170 motif at the start of the activation loop, promoting a "DFG-out" conformation. Some other inhibitors bind only in the purine site, with p38α remaining in a "DFG-in" conformation. We now demonstrate that selectivity pocket compounds prevent MKK6-dependent activation of p38α in addition to inhibiting catalysis by activated p38α. Inhibitors using only the purine site do not prevent MKK6-dependent activation. We present kinetic analyses of seven inhibitors, whose crystal structures as complexes with p38α have been determined. This work includes four new crystal structures and a novel assay to measure K_d for nonactivated p38α. Selectivity pocket compounds associate with p38α over 30-fold more slowly than purine site compounds, apparently due to low abundance of the DFG-out conformation. At concentrations that inhibit cellular production of an inflammatory cytokine, TNFα, selectivity pocket compounds decrease levels of phosphorylated p38α and β. Stabilization of a DFG-out conformation appears to interfere with recognition of p38α as a substrate by MKK6. ATP competes less effectively for prevention of activation than for inhibition of catalysis. By binding to a different conformation of the enzyme, compounds that prevent activation offer an alternative approach to modulation of p38α.

Excessive production of TNFα is involved in the pathogenesis of rheumatoid arthritis, Crohn's disease, inflammatory bowel disease, and psoriasis. The protein kinase p38α has been identified as the molecular target for pyridinylimidazoles (such as SB203580), which block the secretion of TNFα from monocytes stimulated by bacterial lipopolysaccharide (*1*, *2*). Modulation of p38α is a target for the treatment of several inflammatory diseases (*3*). In animal models and isolated cells, a range of stimuli leads to activation of p38α by phosphorylation at residues Thr180 and Tyr182, which are located in a region known as the activation loop (*4*, *5*). Two protein kinases, MKK3 and MKK6, specifically activate p38α in isolated enzyme assays and in vivo (*6*, *7*). There is a report of autophosphorylation of p38α in a TAB1-dependent process (*8*).

Crystal structures have been reported for nonphosphorylated p38α (*9*) and a phosphorylated isoform, p38γ (*10*). The kinase catalytic domains are comprised of an N-terminal lobe, followed by a hinge or linker region (around seven residues)

and then a C-terminal lobe. The flexibility of the hinge allows changes in the relative positions of the two lobes. The catalytic site is at the interface between the lobes, with amino acid residues from both lobes contributing to the ATP-binding site. Key conserved residues in p38α (*11*) include Lys53 (ammonium interacts with α- and β-phosphates of ATP), Glu71 (carboxylate interacts with ammonium of Lys53), Asp168 (carboxylate interacts with Mg^{2+} chelated to ATP), and Asp150 (catalytic base). Glu71 is located on the C-helix within the N-terminal lobe. By analogy to the crystal structure of p38γ with an ATP analogue (*10*), the main-chain amides of His107 and Met109 in the hinge region are expected to form hydrogen bonds with the purine moiety of ATP. The activation loop has relatively high mobility in many p38 crystal structures, so that its position sometimes cannot be resolved. Three-dimensional structures have been determined for nonactivated p38α complexed with peptides from an activating kinase, MKK3b, and a substrate, MEF2A (*12*). Each peptide binds in the same region of the C-terminal lobe, known as the docking groove, which includes the side chains of Ile116 and Gln120.

The catalytic Asp150 in p38α is preceded by an Arg residue, which is a feature found in many protein kinases (*11*). Across this enzyme family, activation loop phosphorylation often increases the catalytic rate constant (k_{cat})[1] and the affinity for ATP (*13*, *14*). In p38α, phospho-Thr180 is expected to dock onto basic side chains in both lobes (including Lys66, Lys67, Arg70 in the N-terminal lobe, and

Arg149 and Arg173 in the C-terminal lobe). By analogy to p38γ (*10*), these interactions may cause closure of the active site cleft, due to a 20° change in the angle between the lobes after phosphorylation and binding of ATP.

Most synthetic protein kinase inhibitors bind in a site that is used by the purine of ATP (*14*, *15*). The compounds form up to three hydrogen bonds in the pattern donor, acceptor, donor, in cis, with main-chain amides. Several classes of p38α inhibitors form a hydrogen bond with the amide NH of Met109 (*2*). Some closely approach the side chain of Thr106. Site-directed mutagenesis and isoform specificity highlight the importance of this residue in determining compound selectivity (*1*, *16*). Thr106 has been referred to as the "gatekeeper" of an adjacent site involving Glu71 and Asp168, which is sometimes called the selectivity pocket.

A drug discovery project in AstraZeneca aims to develop inhibitors of p38α. During the optimization of lead compounds, structures were extended from the purine site, beyond the gatekeeper and into the selectivity pocket, which could be enlarged by displacement of Phe169 (*17*). Our crystallography data led to a proposal that a molecular fragment could bind in the selectivity pocket, while leaving the purine site empty (P. J. Jewsbury and R. A. Pauptit, unpublished results). This was verified by X-ray studies, and inhibition of catalysis was found to occur. ^{15}N,^{1}H TROSY NMR was used to compare the binding of such selectivity pocket compounds with that of adenosine, which binds in the purine site. Occupancy of each site showed characteristic shifts in p38α amide resonances, and in the case of weakly binding ($K_d > 10^{-5}$ M) ligands, the exchange kinetics were fast for the purine site ligands, as expected, but slow or intermediate for the selectivity pocket ligands, implying comparatively slow binding of these compounds. We aimed to find more p38 inhibitors, which bound outside the purine site. Known inhibitors were selected that did not fit with the purine site pharmacophore described above. Diarylureas (*18*) satisfied these criteria and gave NMR data consistent with binding in the selectivity pocket. This binding mode is confirmed by X-ray crystallography for the pyrazolourea described in the current paper. We also show that concentrations of selectivity pocket compounds that decrease cellular synthesis of TNFα unexpectedly lead to decreased phosphorylation of p38 itself. Inhibitors of kinase activity were expected to decrease phosphorylation only of downstream substrates, not the target protein.

Pargellis et al. (*19*) published crystal structures where the selectivity pocket (referred to as an "allosteric site") of p38α was occupied, either by a pyrazolourea or by BIRB796.

BIRB796 and analogues associate with p38α over 100-fold more slowly than a compound that is likely to use only the purine site, SK&F 86002 (*19*, *20*). This slow binding appears to be linked with displacement of the Phe169 side chain, which is part of a conserved DFG sequence at the start of the activation loop, where selectivity pocket compounds promote a change from a DFG-in to a DFG-out conformation. BIRB796 decreases sorbitol-stimulated phosphorylation of p38 in isolated cells (*21*). Although the compound exhibits selectivity against a panel of 14 other protein kinases (*19*), those predominantly responsible for the phosphorylation of p38α (MKK6 and MKK3) were not tested. It is possible, therefore, that the reduced levels of phosphorylated p38 are due to BIRB796 associating with upstream kinases.

The current work focuses on mechanistic studies of seven p38α inhibitors whose binding modes have been established by X-ray crystallography (Figure 1). Four new crystal structures are presented, along with a novel assay to measure K_d for nonactivated p38α and methods to characterize compounds that act by binding to a substrate and preventing its phosphorylation. Inhibitors were selected to include those that bind in the purine site alone, in the selectivity pocket alone, and in a mode that extends across both sites. The compounds that occupy the selectivity pocket are shown to prevent MKK6-dependent activation by binding to p38α.

EXPERIMENTAL PROCEDURES

Materials. Expression and purification of human recombinant p38α are described in Supporting Information. The Division of Signal Transduction Therapy, University of Dundee, supplied fusion proteins of glutathione transferase with nonactivated p38δ (residues 1−365) and glutathione transferase with activated MKK6 (residues 2−334). The following compounds were synthesized at AstraZeneca, Alderley Park, as previously described: SB203580 (*1*), a 4-anilinoquinazoline (*22*), BIRB796 (*19*), a morpholinopy-ridyl-substituted anilinoquinazoline (MPAQ, *17*), a pyrazo-lourea (*18*), a pyridinylimidazole (*23*), a ureidoquinazoline (*24*), Ro3201195, and another pyrazoloamine (*25*). A quinoxaline was made by A. J. G. Baxter (unpublished method) at AstraZeneca, Charnwood. Structures of these compounds are shown in Figure 1 or in Supporting Information.

Phosphorylation of p38α. Nonphosphorylated p38α (24 μM) was incubated with 1 mM ATP, 480 nM MKK6, 50 mM MOPS, pH 7.4, 10 mM MgCl$_2$, 1 mM dithiothreitol, and 0.001% (v/v) Tween 20 at room temperature for 50 min. Products were analyzed by mass spectrometry and using an ELISA kit (Biosource) in order to ensure that p38α was largely phosphorylated at both Tyr180 and Thr182. MKK6 was removed using a Resource Q (Amersham Biosciences) column, and doubly phosphorylated p38α was purified by gel filtration as described in Supporting Information.

In the procedures described below, concentrations of p38 were estimated as total protein divided by M_r. These values were within 2-fold of those calculated by fitting dose−response equations for tight-binding inhibitors (see below), implying that the proteins were over 50% pure and active. Nonphosphorylated p38α lacked phosphates on Tyr180 and Thr182 as judged by the lack of cross-reactivity with specific antibodies and by mass spectrometry.

Determination of Crystal Structures. For each compound, 200 μM nonphosphorylated p38α and 1 mM inhibitor were
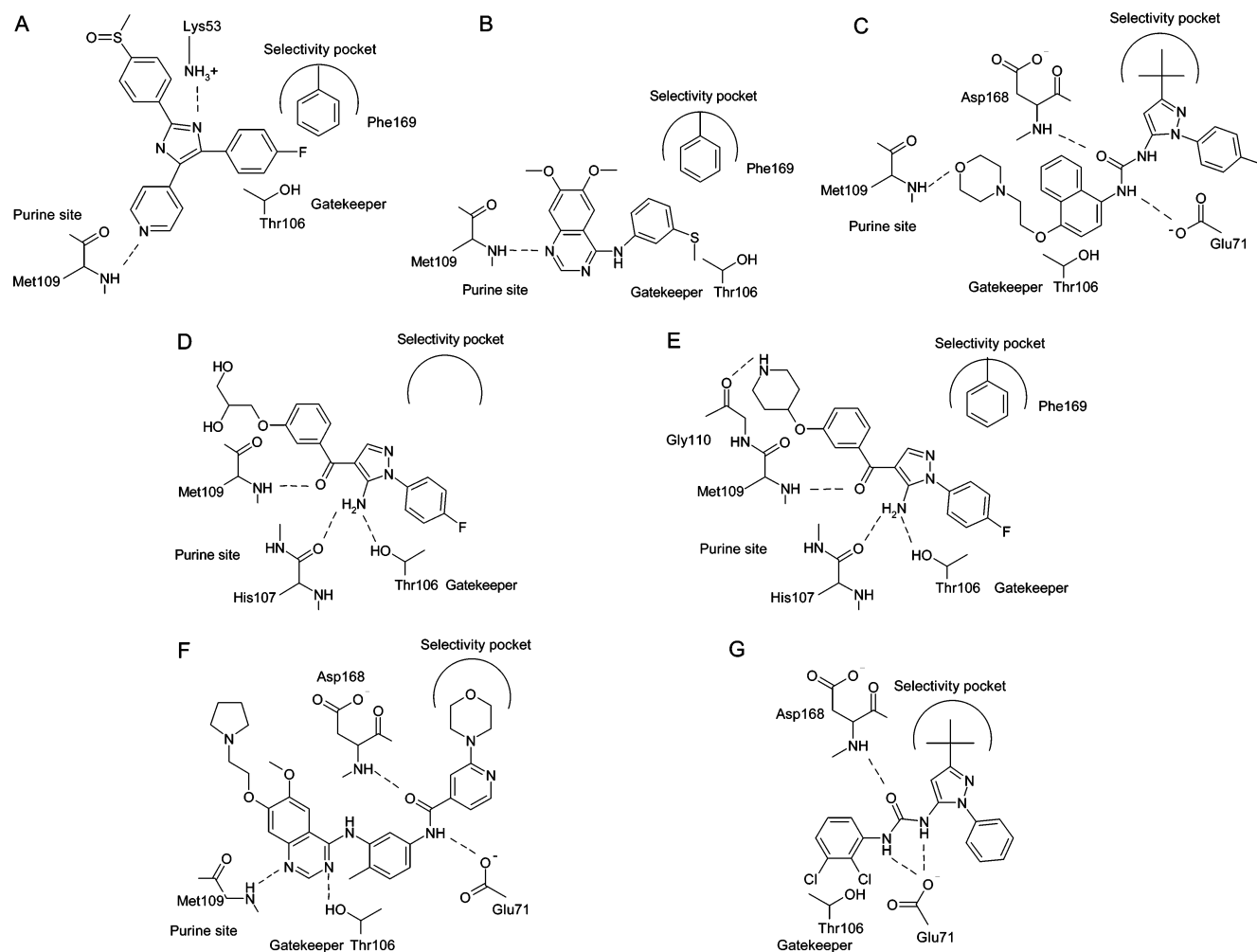

FIGURE 1: Chemical structures with schematic binding modes for p38 inhibitors: (A) SB203580, (B) anilinoquinazoline, (C) BIRB796, (D) Ro3201195, (E) pyrazoloamine, (F) MPAQ, and (G) pyrazolourea. Hydrogen bonds are shown as dashed lines. The conformation of p38α changes according to the identity of the inhibitor.

incubated for 30 min at 4 °C and then centrifuged (14000 rpm, 4 °C, 15 min) immediately prior to using the supernatant. Each complex was crystallized by hanging drop vapor diffusion over a screen of 6−10% (w/v) poly(ethylene glycol) 5000 monomethyl ether or 12−16% (w/v) poly(ethylene glycol) 1500 and cacodylate or malate/imidazole buffers, pH 6−7. Crystals generally appeared after 24−72 h and reached maximum size (500 × 50 × 50 μm for needle crystals and 400 × 200 × 200 μm for block-shaped crystals) after 7 days. Crystals were cryoprotected by serial dipping (approximately 30 s) in reservoir solution with 5−20% (v/v) additional glycerol in 5% steps. Crystals then were cooled rapidly to 100 K prior to data collection.

Diffraction data for MPAQ, the pyrazolourea, and pyrazoloamine in complex with p38α were collected on an ADSC CCD detector at the Synchrotron Radiation Source, Daresbury, U.K. (station 9.6, λ = 0.87 Å) at 100 K. Data from Ro3201195 were collected at AstraZeneca, Alderley Park, on a Marresearch DTB image plate detector mounted on a Bruker-Nonius FR591 rotating anode operated at 6 kW using Cu Kα radiation (λ = 1.542 Å). All data were processed using MOSFLM (*26*), and programs from the CCP4 suite were used for data reduction and structure determination. Structures were solved by molecular replacement using AMoRe (*27*), with in-house p38α complexes as trial models. The first in-house structure was solved using murine p38α

(PDB code 1P38; *9*) as the search model. The protein complex models were refined using Refmac5 (*28*) and rebuilt using Quanta2000 (Accelrys). Data collection and refinement statistics are given in Table 1.

NMR Studies. Recombinant human p38α with an amino-terminal His$_6$ tag was uniformly labeled with ^{15}N and ^{2}H, or ^{15}N, ^{13}C, and ^{2}H ·as described in Supporting Information. Samples for NMR were prepared at 120−800 μM protein concentration in buffer containing 50 mM HEPES, pH 7.5, 50 mM NaCl, 5 mM tris(2-carboxyethyl)phosphine hydrochloride, 0.1 mM EDTA, 0.02% (w/v) NaN$_3$, and 5% (v/v) D$_2$O for use with a cryogenic probe or in buffer containing 50 mM sodium phosphate, pH 7.4, 50 mM NaCl, 5 mM DTT, 0.1 mM EDTA, 0.02% (w/v) NaN$_3$, and 5% (v/v) D$_2$O for use with an ambient temperature probe. For ligand binding studies at reduced pH, the same sodium phosphate buffer was used, but at pH 6.0. Data were acquired at 25 °C on 600 MHz Varian Inova or Bruker Avance spectrometers equipped with triple-resonance cryogenic and ambient temperature pulsed-field z-gradient probes. Backbone resonance assignments were obtained mainly from analysis of data sets acquired on samples of ^{15}N,^{13}C,^{2}H-p38α using 3D (HNCA, HNcoCA, HNCO, HNcaCO, HNcaCB, HNcocaCB; *30*) and 4D (HNCACO, HNCOCA, HNCOCA-sim, N,N-NOESY; *29*) TROSY-based experiments and will be reported in detail elsewhere. A 3D ^{15}N-separated NOESY-HSQC data set was

Table 1: X-ray Data and Refinement Statistics

	inhibitor			
	Ro3201195	pyrazoloamine	MPAQ	pyrazolourea
space group	$P2_12_12_1$	$P2_12_12_1$	$P2_12_12_1$	$P2_12_12_1$
cell constants (Å)	64.8, 74.7, 76.9	65.2, 75.2, 77.8	66.3, 75.8, 78.1	59.0, 67.1, 87.7
resolution (Å)	19.4−2.8	24.5−2.1	50.6−2.2	53.5−2.25
completeness (%)	89.5	93.5	87.5	95.7
unique reflections	9604	22912	17815	17097
multiplicity (%)	2.3	2.5	2.4	2.6
R_{merge}[a]	0.11	0.062	0.035	0.078
R_{value} (%)[b]	21.8	21.7	21.8	21.7
R_{free} (%)[c]	29.6	26.5	25.0	30.2
RMSD from ideal values				
bond lengths (Å)	0.013	0.009	0.014	0.016
bond angles (deg)	1.551	1.134	1.447	1.640
average B values (Å^2)				
protein, all atoms	29.1	28.4	27.7	25.8
ligand	30.7	27.8	26.0	17.0
solvent	32.3	28.4	27.4	22.0

[a] $R_{merge} = \sum_{hkl}[(\sum_i|I_i - \langle I\rangle|)/\sum_i I_i]$. [b] $R_{value} = \sum_{hkl}||F_o| - |F_c||/\sum_{hkl}|F_o|$. [c] R_{free} is the cross-validation R factor computed for the test set of 5% of unique reflections.

also acquired on an 800 MHz Bruker Avance spectrometer. Ligand interaction studies were performed using a chemical shift perturbation approach: Compounds dissolved at 0.1 M in DMSO were titrated into 500 μM samples of ^{15}N,^{2}H-p38α, and at each compound concentration, a ^{1}H−^{15}N TROSY correlation spectrum was acquired with (t_1, t_2) acquisition times of 53 (^{15}N) and 85 (^{1}H) ms. NMR spectra were processed using NMRPipe (*31*) and analyzed using NMR-View (*32*).

Measurement of Binding Affinity. A Biacore 3000 was used to monitor binding interactions during inhibition in solution assays (ISAs; *33*). A target definition compound (see Supporting Information) that was known to compete with test compounds in binding to p38α was immobilized on the sensor chip. The enzyme was incubated with various concentrations of test compounds for 30 min and then allowed to flow over the sensor. Unbound p38α associated with the target definition compound giving a signal, which could be related to the free concentration. Dose−response data were analyzed to estimate K_d values (eq 1 or 3, where $K_i' = K_d$), because competition by the target definition compound did not cause a significant shift in the midpoint.

The target definition compound was immobilized by amine coupling onto a research-grade CM-5 chip using 7 min injections of a mixture of 11.5 mg/mL *N*-hydroxysuccinimide with 75 mg/mL 1-ethyl-3-(3-dimethylaminopropyl)carbodiimide hydrochloride, followed by 400 μM compound in 10 mM HEPES, pH 7.4, 0.15 M NaCl, 3.4 mM EDTA, 0.005% (v/v) surfactant P20, 4% (v/v) dimethyl sulfoxide, and finally 1 mM ethanolamine, pH 8.5, at a flow rate of 5 μL/min. Immobilization levels typically were around 3000 resonance units. A reference flow cell was prepared without the target definition compound. All measurements used a flow rate of 20 μL/min, and subtractions were made to eliminate refractive index change and injection noise. Surface regeneration was achieved by injecting 5 μL of 100 mM NaOH. The chip was calibrated with either nonphosphorylated or phosphorylated p38α using a report point of 60 s, when response was increasing linearly with time. Response was linear up to at least 400 nM protein. K_d measurements were performed at 10−50 nM p38α. More details are given in Supporting Information.

Catalysis by Activated p38α. Each 50 μL reaction contained 50 mM Tris-HCl, pH 7.4, 0.1 mM EGTA, 0.1 mM sodium orthovanadate, 0.001% β-mercaptoethanol, 10 nM phosphorylated p38α, 10 μM ATP, 0.1 μCi [γ-^{33}P]ATP, 10 mM MgCl$_2$, and 9 μM myelin basic protein (MBP). The inhibitor was preincubated with the enzyme and MBP, typically for 60 min, and then the assay was started by addition of ATP. Reactions proceeded for 60 min and then were stopped using 10% (w/v) trichloroacetic acid prior to filtration onto GF/C filter plates. Incorporation of ^{33}P was determined following the addition of 30 μL of Optiscint-0.

Measurement of Binding Kinetics. For most compounds, association rate constants were measured by following the decrease in fluorescence accompanied by displacement of a pyridinylimidazole reporter molecule (IC$_{50}$ approximately 40 nM against activated p38α; see Supporting Information). Excitation and emission were respectively at 310 and 394 nm. Enzyme (30 nM) and 60 nM fluorescent probe were equilibrated for 20 min in 50 mM HEPES, pH 7.4, 150 mM NaCl, and 20 mM MgCl$_2$ before addition of test compound at up to 0.48 μM. For the measurement of dissociation rate constants, 30 nM enzyme and 30 nM compound were equilibrated for 45 min before addition of 10 μM reporter and following the increase in fluorescence for up to 10 h. Experiments at various concentrations of fluorescent reporter indicate that its association and dissociation were too fast to measure and that its presence at these concentrations does not perturb the kinetics of the test compounds. For the binding of BIRB796, the fluorescence of the compound itself was monitored directly (excitation at 310 nm, emission at 394 nm). Data were analyzed as described below, using GraFit (*34*).

Cell-Based Assays. THP1 cells were incubated with test compound in 0.1% (v/v) dimethyl sulfoxide for 30 min at 37 °C before being stimulated with 50 μg/mL lipopolysaccharide (LPS) for either 6 h (TNFα release experiments) or 30 min (p38α pathway activation experiments). Supernatants were removed and assayed for TNFα by ELISA. For measurement of p38, the cells were pelleted by centrifugation and then lysed with 20 mM Tris-HCl, pH 7.5, 150 mM NaCl, 1 mM EDTA, 1 mM EGTA, 1% (v/v) Triton X-100, 2.5 mM sodium pyrophosphate, 1 mM β-glycerophosphate, 1

mM Na_3VO_4, 1 $\mu g/mL$ leupeptin, and 1 mM phenylmethane-sulfonyl fluoride. ELISA then was used to measure either the sum of phosphorylated p38α and β or the level of total p38α (which varied by less than 2-fold within each dose—response study). Results were analyzed as a ratio of phosphorylated α plus β to total p38α in order to adjust for differences in yield.

MKK-Dependent Phosphorylation of p38. For phosphorylation of p38α, each 50 μL reaction contained 50 mM MOPS, pH 7.4, 0.001% (v/v) Tween 20, 10 mM $MgCl_2$, 1 mM dithiothreitol, 20 nM p38α, 1 μM ATP, 0.2 nM MKK6 or 10 nM MKK3, and inhibitor in 1% (v/v) dimethyl sulfoxide. There was a 30 min preincubation of p38α with compound before starting the assay by addition of MKK. The reactions proceeded for 15 min and were stopped using 20 mM EDTA. A 10 μL aliquot was used to determine phosphorylated p38α using ELISA.

Phosphorylation of p38δ was detected radiometrically using 500 nM p38δ, 1 μM ATP, 0.1 μCi of 5′-[γ-^{33}P]ATP, 10 mM $MgCl_2$, and 10 nM MKK6. Reactions were allowed to proceed for 40 min before stopping using 10% (v/v) trichloroacetic acid, filtration, and counting as described above.

Data Analysis. For all experiments, there were linear relationships between signal and enzyme concentration or time. Equations were fitted to data by unweighted nonlinear regression using GraFit (*34*). Identification of the most suitable equation was assisted by an *F*-test (*35*). All reported values are geometric means from replicate measurements, with 95% confidence intervals estimated as being within a factor of 2 for isolated protein assays or a factor of 3 for cell-based assays. When fitting equations to data, the parameter values, *x*, for midpoints, or concentrations of binding sites, were replaced by $10^{\log x}$. This does not change the magnitude of the best-fit value for *x* and may allow more realistic estimation of confidence intervals (*36*). Fitting to some data sets required addition of a background term to allow for apparent partial effects at saturating concentrations of compound.

(a) Inhibition by Binding to Enzyme and ISA. If there is no depletion of inhibitor ($[I]_t \approx [I]$, that is, total and free inhibitor concentrations are approximately equal), then rate is given by

$$v = v_0/(1 + [I]_t/K_i') \tag{1}$$

where v_0 is the uninhibited rate and K_i' is the apparent inhibition constant (*37*). When the compound follows competitive kinetics with respect to the varied substrate

$$K_i' = \frac{K_{is}(K_m + [S]_t)}{K_m} \tag{2}$$

where K_{is} is the inhibition constant when $[S]_t \ll K_m$. If there is depletion of inhibitor (known as tight-binding inhibition), then

$$v = [v_0/2]\Big[(1 - K_i'/[E]_t - [I]_t/[E]_t) + \\ \sqrt{[K_i'/[E]_t + [I]_t/[E]_t - 1]^2 + 4K_i'/[E]_t}\Big] \tag{3}$$

where $[E]_t$ is the concentration of binding sites (*38*). The midpoint of the dose—response curve is

$$IC_{50} = K_i' + [E]_t/2 \tag{4}$$

because IC_{50}, K_i', and $[E]_t/2$ are respectively total, free, and bound inhibitor concentrations. In ISA, v_0 corresponds to response at zero inhibitor and K_i' is K_d.

(b) Binding Kinetics. The following relationship was fitted to data for association of most test compounds:

$$F_t = (F_0 - F_\infty)e^{-k_{obs}t} + F_\infty \tag{5}$$

where F is fluorescence and the subscripts refer to time 0, ∞, and *t*. The observed rate constant is given by

$$k_{obs} = k_{on}[I] + k_{off} \tag{6}$$

Fitting of this equation allowed estimation of k_{on} and k_{off}. The values for k_{off} were consistent with those from dissociation of test compounds, which were calculated from the relationship

$$F_t = (F_\infty - F_0)(1 - e^{-k_{off}t}) + F_0 \tag{7}$$

For BIRB796, no reporter was used so that eq 7 was fitted to association data and the rate constant corresponded to k_{obs} in eq 6.

(c) Inhibition by Binding to Substrate. Dose—response equations are derived in the Appendix. The observed rate, v, is given by eq A20, where the free inhibitor concentration is determined by eq A12 and the magnitude of K_i' is as shown in eq A18. IC_{50} again is a function of free and bound inhibitor concentrations, as derived in eq A23. These compounds were characterized when $[S] \ll K_m$, so that there is an approximately linear relationship between rate and free substrate concentration. Under these conditions

$$IC_{50} = K_{is} + [S]_t/2 \tag{8}$$

(d) Cell-Based Assays. The following equation was fitted

$$y = \frac{y_0}{1 + [I]_t^{sl}/IC_{50}^{sl}} \tag{9}$$

where y_0 is the uninhibited control and sl is the slope when $[I]_t = IC_{50}$. An equation where sl was fixed to 1 also was fitted to the data, and selection of the most suitable equation was assisted by an *F*-test (*35*).

RESULTS

Characteristics of p38α before and after Activation. Binding assays are required to characterize the association of compounds with nonactivated p38α, because it has no detectable phosphotransferase activity. A BIAcore ISA protocol has been developed for this purpose (Supporting Information). Activation results in a decrease of over 7-fold in K_d(ATP) and an increase of over 10000-fold in k_{cat} for MBP (Table 2). These consequences are similar to those reported by Frantz et al. (*5*). For activated p38α, K_m(ATP) is over 5-fold lower than K_d(ATP), which indicates accumulation of intermediates after formation of the enzyme—ATP complex (*39*). K_m(ATP) has been reported between 23 and 200 μM, according to the identity of the substrate (*4, 40, 41*). The observed value of k_{cat} (Table 2) is close to a

Table 2: Kinetic Characteristics of p38α[a]

	nonactivated p38α	activated p38α
K_d(ATP) (μM)	>10000	1300
K_d(ADP) (μM)	>10000	1100
k_{cat} (s^{-1})	$<1.2 \times 10^{-5}$	0.13
K_m(ATP) (μM)	ND	220
K_m(MBP) (μM)	ND	10

[a] K_d values were estimated using ISA. K_m for ATP was determined at 100 μM MBP. K_m for MBP was measured at 1 mM ATP. ND, not determined, because catalytic activity was below the levels of detection.

previous value of 0.08 s^{-1} (*40*). The value of K_d(ADP) is similar to a published K_{is}(ADP) = 570 μM (*41*).

X-ray Crystal Structures of Enzyme−Inhibitor Complexes. The previously published structures with SB203580 (PDB: 1A9U) (*42*) and an anilinoquinazoline (PDB: 1DI9) (*22*) show that these compounds do not occupy the selectivity pocket and that p38α is in a DFG-in conformation (Figure 1A,B). With each compound, the phosphorylation sites, Thr180 and Tyr182, are ordered and oriented toward solvent. The docking groove in the complex with SB203580 is ordered, although the temperature factors (*B* values) are high. For the anilinoquinazoline, the docking groove is partially ordered, with Ile116 and some of Gln120 being localized. The previously reported BIRB796 structure (PDB: 1KV2) (*19*) indicates binding in both the purine and selectivity pockets, with the protein adopting a DFG-out conformation (Figure 1C). The activation loop beyond Phe169 is disordered, and residues 170−184 are not localized. The docking groove also is disordered and the positions of residues 115−122 are not defined.

The structure of the complex with Ro3201195 now has been determined (Figures 1D and 2A). The compound is bound only in the purine site, where the keto O accepts a hydrogen bond (2.9 Å) from the main-chain amide of Met109 and, like SB203580, a fluorophenyl ring is close to the gatekeeper. The 5-amino group of the inhibitor forms one hydrogen bond (2.9 Å) with the side-chain oxygen of Thr106 and another with the main-chain C═O of His107 (3.1 Å). Ro3201195 does not enter the selectivity pocket. The protein, however, is in a DFG-out conformation. This may be linked to an interaction between the side chains of Glu71 and Asp168 (2.2 Å between carboxyl oxygens) at the start of the activation loop. There must be protonation of one of these groups, which is favored by the low pH of 6.2. These carboxyl oxygens are at least 4.5 Å apart in each of the other six crystal structures. In isolated enzyme and cell-based assays (see below), Ro3201195 exhibits similar characteristics to other compounds that do not use the selectivity pocket, suggesting that it does not induce predominance of a DFG-out conformation in solution at physiological pH. In this complex, residues 173−181 are disordered, and only one phosphorylation site, Tyr182, can be localized. Residues 119−121, including part of the docking groove, also are disordered.

The pyrazoloamine is related to Ro3201195, with the dihydroxypropane substituent being replaced by a piperidyl group. The structure of the complex with p38α shows that the compound occupies only the purine site and the protein is in a DFG-in conformation (Figures 1E and 2B). Again, there are hydrogen bonds with Met109 (2.9 Å), Thr106 (2.9 Å), and His107 (3.1 Å). Additionally, the ring nitrogen of

the piperidine is hydrogen bonded (3.3 Å) to the main-chain oxygen of Gly110 in the purine site. This piperidine has an axial linkage to the 3-oxophenyl group of the ligand and has been refined in a boat conformation. In contrast to the complex with Ro3201195, there is no interaction between the side chains of Glu71 and Asp168 (5.0 Å between carboxyl oxygens). The phosphorylation sites are not visible in the electron density as residues 173−183 are missing, and the docking groove is included in the model, but poorly defined.

MPAQ occupies both the purine site and selectivity pocket (Figures 1F and 2C). There has been a preliminary report of an unrefined structure (*17*). Now, a fully refined structure is presented. The quinazoline N1 accepts a hydrogen bond (3.1 Å) from the main-chain amide of Met109, while N3 donates a hydrogen bond (2.9 Å) to the side-chain O of gatekeeper Thr106. An amide in the inhibitor forms a trans hydrogen-bonding arrangement with Glu71 (2.8 Å) and Asp168 (3.1 Å), which is similar to that for the urea of BIRB796. The morpholine is located in a hydrophobic pocket, bounded by Leu74, Met78, Val83, Ile84, Ile141, and Ile166. This part of the inhibitor has displaced the side chain of Phe169 (DFG-out conformation) into the ATP pocket, where is forms nonpolar contacts with Leu167. The pyrrolidinium group of the inhibitor forms an intramolecular hydrogen bond (2.8 Å) with the previous O and extends into solvent. The docking groove residues 118−120 are not visible in the electron density, nor are residues 171−182 of the activation loop.

The pyrazolourea does not use the purine site, binding only in the selectivity pocket (Figures 1G and 2D). It forms three trans hydrogen bonds, two with the same oxygen atom in the carboxylate of Glu71 (both 3.0 Å) and one with the main-chain NH of Asp168 (2.9 Å). The *tert*-butyl group displaces the side chain of Phe169 from the selectivity pocket, interacting with Leu74, Leu75, Met78, Val83, Ile84, Ile141, and Leu167. Phe169 again is in the ATP site, close to Leu167 and the dichlorophenyl moiety of the inhibitor, which is in contact with the gatekeeper. The activation loop main-chain conformation is defined, with higher flexibility for the side chains. The loop is folded in a closed conformation, with Thr180 oriented toward the body of the protein and Tyr182 pointing toward solvent. Residues 115−124, including side chains from the docking groove, are disordered. Overall, this structure is similar to that for a weaker analogue (*19*).

Characterization of Binding Kinetics. Previous results indicate that compounds inducing a DFG-out conformation bind over 200-fold more slowly than SK&F 86002, which probably associates with a DFG-in conformation (*19, 20*). It has not been shown whether slow binding occurs as a single kinetic step or involves rapid formation of initial complexes, followed by a slower transition to tighter binding. A one-step mechanism would be consistent with selecting DFG-out from existing conformations, whereas two steps suggest induction of a DFG-out conformation after binding. We now investigate this question using nonactivated p38α and characterize additional compounds. Slow tightening after faster formation of an initial complex leads to saturation kinetics, with the half-maximal rate occurring at an inhibitor concentration, which approximates to the K_d for the initial step (*38*). Conversely, a linear relationship between association rate and inhibitor concentration, extending to levels well above the final K_d value, indicates that there is no accumula-
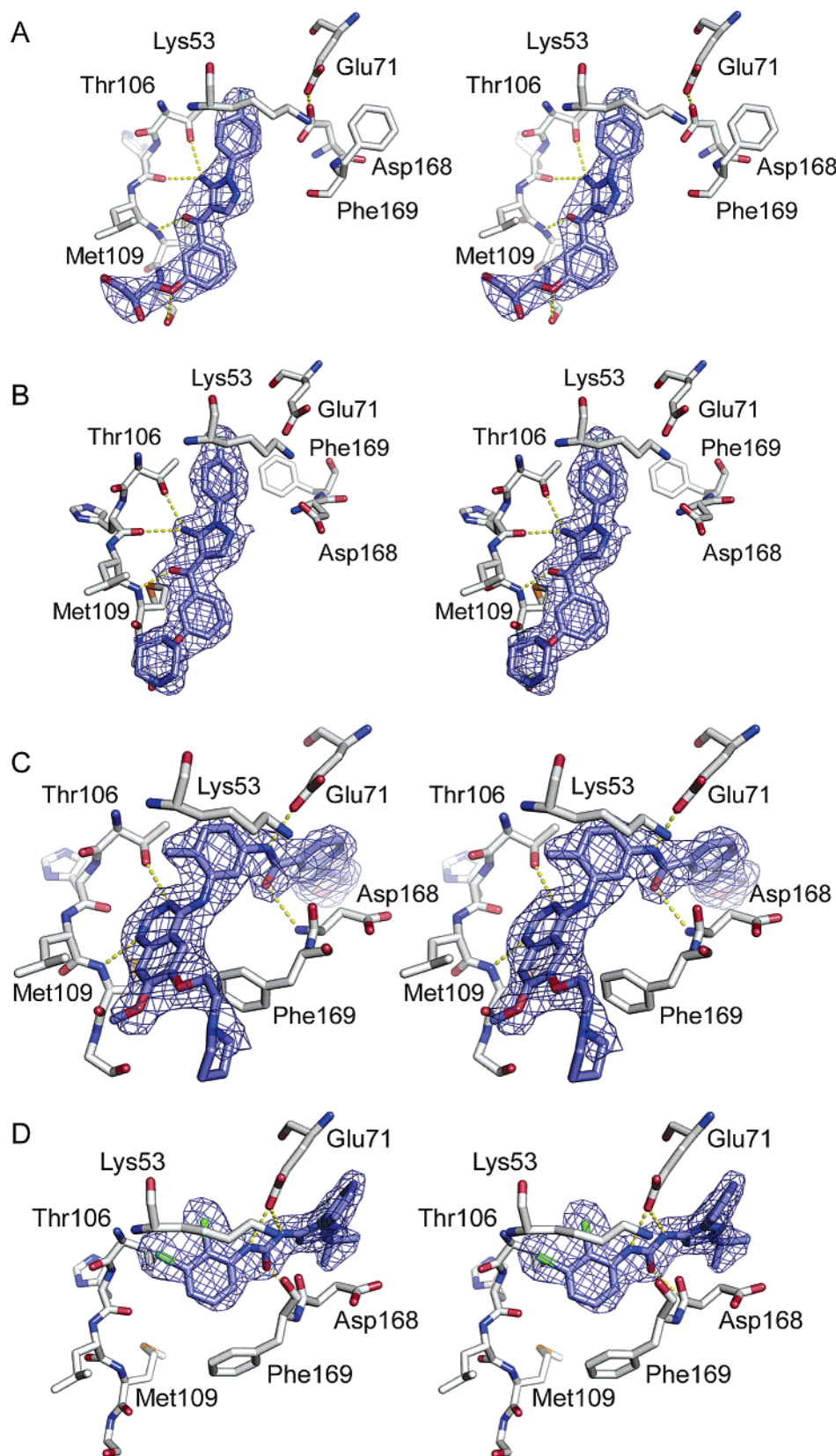
FIGURE 2: Relaxed eye stereoviews of the binding sites for Ro3201195 (A), pyrazoloamine (B), MPAQ (C), and pyrazolourea (D) bound to p38α. The refined $2F_o - F_c$ electron density maps covering the bound ligands are contoured at 1.0σ.

tion of intermediate prior to the final complex and is consistent with conversion between binding and nonbinding conformations being more rapid than the association step.

Association rate constants were measured by monitoring the time courses of fluorescence changes, which followed single exponential kinetics (Figure 3A) and allowed estimation of the observed rate constant, k_{obs}. Use of eq 6 to analyze a plot of k_{obs} against inhibitor concentration gave the values of k_{on} and k_{off} (Figure 3B). The magnitude of k_{off} was estimated by extrapolation, which limited precision. More
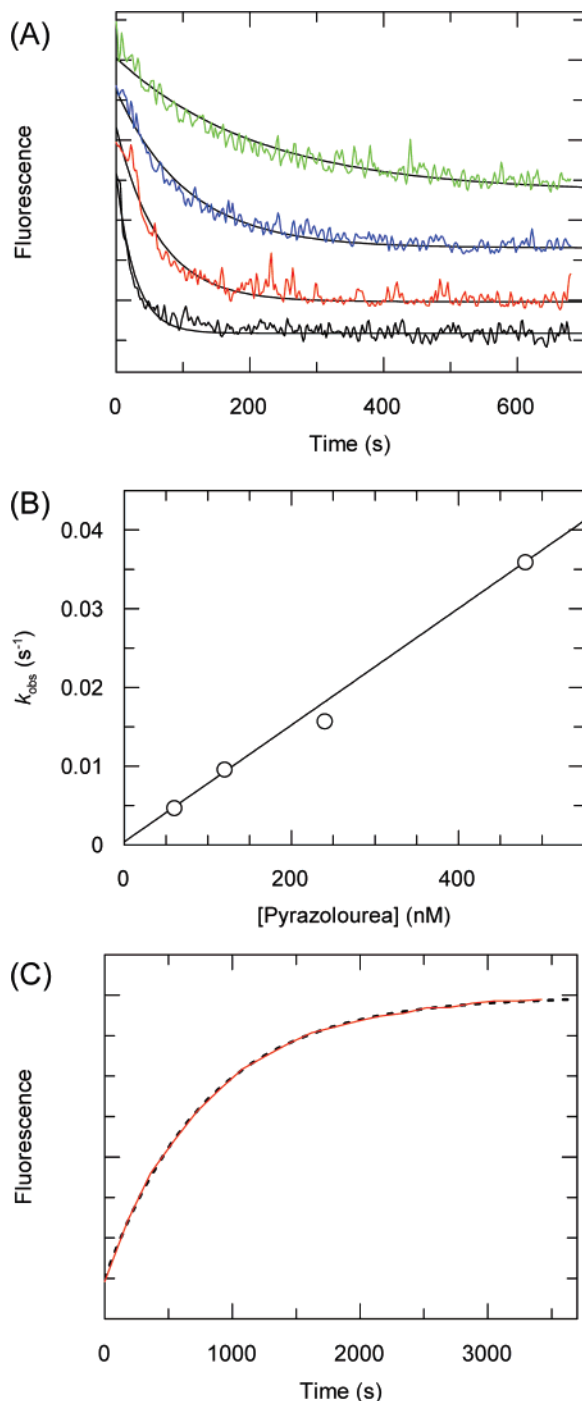
(A)

(B)

(C)

FIGURE 3: Measurement of association and dissociation rate constants. Details are in Experimental Procedures. (A) Time courses for displacement of the fluorescent reporter from nonactivated p38α by the following concentrations of the pyrazolourea: green line, 60 nM; blue line, 120 nM; red line 240 nM; black line, 480 nM. The smooth black lines were calculated using the best-fit values of k_{obs} from eq 5. The data and lines are offset to improve clarity. (B) A plot of the k_{obs} values from (A). The best-fit line from eq 6 is shown as $k_{on} = 7.4 \times 10^4$ s^{-1} M^{-1} (95% CIs within 2-fold) and $k_{off} = 4 \times 10^{-4}$ s^{-1} [95% CIs $\approx$ (0.4−40) $\times$ 10^{-4} s^{-1}]. (C) Time course for displacement of the pyrazolourea by the reporter (red line). The dashed black line was calculated using the best-fit $k_{off} = 1.3 \times 10^{-3}$ s^{-1} (95% CIs within 2-fold) for eq 7.

precise values were obtained by following displacement of test compound by a fluorescent reporter (Figure 3C, Table 3). These experiments give a linear relationship between k_{obs} and the concentration of BIRB796 up to 960 nM

Table 3: Association and Dissociation Rate Constants for Nonactivated p38α[a]

	method			
	displacement of reporter		displacement by reporter	
compound	k_{on} (s^{-1} M^{-1})	k_{off} (s^{-1})	k_{off} (s^{-1})	K_d (nM)[b]
	Compounds Using the Purine Site Only			
all[c]	$>5 \times 10^6$	ND[d]	>0.01	ND[d]
	Compounds Using the Selectivity Pocket			
BIRB796[e]	1.3×10^5	$<1 \times 10^{-4}$	ND[d]	<0.8
MPAQ	1.2×10^5	$<5 \times 10^{-3}$	4.0×10^{-3}	33
pyrazolourea	1.1×10^5	8.6×10^{-4}	1.1×10^{-3}	10

[a] Rate constants were measured as described in Experimental Procedures. [b] Calculated as k_{off}/k_{on}, using k_{off} from displacement by reporter. [c] SB203580, anilinoquinazoline, Ro3201195, and pyrazoloamine. [d] Not determined. [e] Values of k_{on} and k_{off} estimated from the concentration dependence of k_{obs}, which was measured by following the fluorescence of BIRB796 with no reporter. K_d calculated from these values, because the dissociation of BIRB796 was too slow for direct measurement.

(see Supporting Information), which is over 1000-fold higher than the K_d value estimated as k_{off}/k_{on} (<0.8 nM). This observation of single-step kinetics is consistent with, but not proof of, a direct binding process. Similar results are obtained at up to 480 nM MPAQ or pyrazolourea, suggesting that the affinity for any initial complex must be at least 14-fold weaker than K_d. The association and dissociation rates for SB203580, the anilinoquinazoline, Ro3201195, and the pyrazoloamine are too fast to measure, in agreement with the results on SK&F 86002 (*19*) and consistent with the pattern that purine site only compounds follow more rapid kinetics (Table 3). The k_{on} for Ro3201195 is typical of that for a DFG-in compound and distinct from that for DFG-out compounds, suggesting that a DFG-in conformation predominates for this complex in solution at this pH. This result is consistent with the compound occupying only the purine site and suggests that the conformation in solution is different from that in the crystal form obtained at lower pH.

The values of K_d estimated from the ratio k_{off}/k_{on} (Table 3) are consistent with those from ISA (Table 4), where BIRB796 exhibits a K_d value, which is below the limit for measurement (approximately 4 nM). The estimated rate constants for BIRB796 are in agreement with those previously published ($k_{on} = 0.85 \times 10^5$ s^{-1} M^{-1}, $k_{off} = 8.3 \times 10^{-6}$ s^{-1}, $K_d = 0.098$ nM; *19*).

The two most potent selectivity pocket compounds (BIRB796 and the pyrazolourea) exhibit similar slow binding behavior with activated p38α in that IC$_{50}$ values (=K_i' + [E]$_t$/2; eq 4) decrease at least 3-fold following preincubation with the enzyme for 30 min. (MPAQ behaved as expected, not giving a shift in IC$_{50}$, because it inhibits only at higher concentrations.) To obtain estimates of steady-state K_i' values (Table 4), preincubations were extended to 120 min, when results were in agreement with those at 60 min. Assays were started with minimal dilution and ensuring that addition of competing ATP would give a less than 2-fold increase in K_i'. Such slow binding kinetics have been seen previously for BIRB796, which exhibited an IC$_{50} = 97$ nM without preincubation and 8 nM after 120 min preincubation (*19*).

NMR Studies on the Binding of Ro3201195 and the Pyrazoloamine. The observation of a DFG-out conformation in the crystal structure of the Ro3201195 complex with p38α

Table 4: Comparison of p38 Inhibitors in Isolated Protein and Cell-Based Assays[a]

	nonactivated p38				activated p38		THP1 cells	
compound	binding K_d (nM)	MKK6/p38α K_i' (nM)	MKK6/p38δ K_i' (nM)	MKK3/p38α K_i' (nM)	binding K_d (nM)	inhibition K_i' (nM)	phospho-p38 IC_{50} (nM)	TNFα IC_{50} (nM)
			Bind in Purine Site Only					
SB203580	9.0	>10000	>10000	140[c]	20	9.0	>10000	64
anilinoquinazoline	19000	>100000	>10000	ND	37000	3800	>50000	>50000
Ro3201195	95	>10000	>10000	470[c]	170	210	>10000	200
pyrazoloamine	490	>10000	>10000	970[c]	590	740	ND	>10000
			Binding Includes Selectivity Pocket					
BIRB796	<0.8[b]	<10[c]	850	33	<1.0	<8	7.7	6.0
MPAQ	37	37[c]	4700	59	38	39	710	1400
pyrazolourea	4.0	6.0	16000	10	3.0	8	60	48

[a] Reported values are geometric means from repeated measurements, with 95% CIs estimated as being within a factor of 2 for isolated protein assays or a factor of 3 for cell-based assays. [b] Calculated as k_{off}/k_{on}. Other K_d values were measured by ISA and, together with K_i' for activated p38, were estimated by fitting to eq 1 or 3. [c] Partial inhibition, with a background of around 20% of the uninhibited rate at saturating concentrations of the test compound. When nonactivated p38 was used as a substrate, K_i' was calculated using eqs A12, A20, and A23. In some cases, depletion of inhibitor by tight binding to the target protein prevented precise estimation of K_d or K_i'. Here, the value is reported as less than the upper 95% CI. IC_{50} values in THP1 cells were estimated using eq 9. ND, not determined.
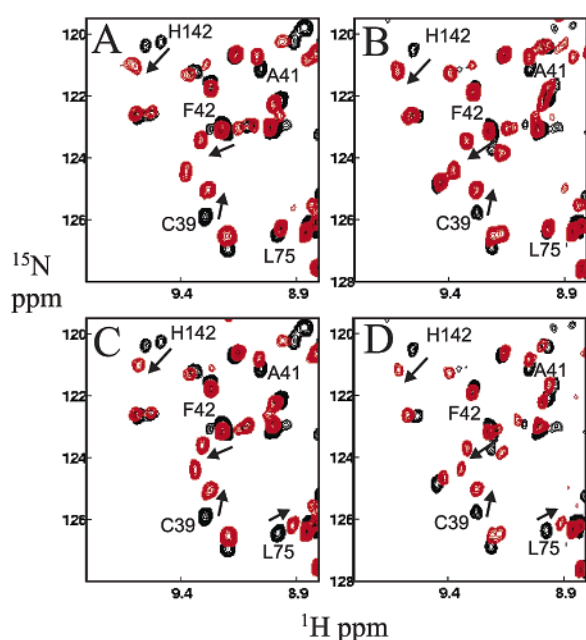

FIGURE 4: NMR spectra of p38α complexed with inhibitors. Selected region of 2D $^1H-^{15}N$ TROSY correlation spectra showing an overlay of inhibitor-bound (red) and free (black) spectra of $^{15}N,^2H$-p38α with Ro3201195 (A and B) and the pyrazoloamine (C and D) at pH 7.4 (A and C) and pH 6.0 (B and D). Chemical shifts are uncorrected for TROSY offset. Concentrations of inhibitor and protein were respectively 600 μM (when present) and 500 μM.

was not expected, since it occupies only the purine site. NMR chemical shift perturbation mapping is a sensitive probe of structural changes in response to ligand binding and was employed to compare the effects of Ro3201195 and the pyrazoloamine analogue at pH 7.5 and 6.0, which is close to the pH of 6.2 used for crystallization. Figure 4 shows regions of the $^1H-^{15}N$ TROSY correlation spectra of p38α in the presence of Ro321195 or the pyrazoloamine. The patterns of backbone amide resonance shifts induced by each compound are similar at each pH value and resemble those observed for other purine site inhibitors. The lack of significant differences between Ro3201195 and its analogue coupled with the rapid binding kinetics (Table 3) suggests that, under these solution conditions, a DFG-in conformation of p38α predominates when complexed with Ro3201195.

A Pyrazolourea Prevents Activation by Binding to p38α. In LPS-treated THP1 cells, three selectivity pocket compounds reduce levels of phosphorylated p38 with IC_{50} values, which are similar those for inhibition of TNFα production (Table 4). These results suggest that the compounds do not only inhibit catalysis by activated p38α, because this would decrease phosphorylation only for proteins that follow in the signaling pathway. Measurements using antibody indicate that this effect is not due to reduction of total p38α levels. Isolated protein assays were developed in order to explore whether changes in phospho-p38α were due to effects on MKK6-dependent activation. At 1 μM ATP with p38α as the substrate, the observed kinetic parameters are $k_{cat} \approx 0.02$ s^{-1} and $K_m = 0.75$ μM, whereas using p38δ, $k_{cat} \approx 0.002$ s^{-1} and $K_m = 1.8$ μM. The K_m for ATP is 1.7 μM. Concentrations of p38 below K_m were used, giving an approximately linear relationship between rate and free p38 concentration. Assay at saturating p38 would reduce the sensitivity to compounds that act by depleting the free substrate.

Binding assays indicate that the pyrazolourea associates with nonactivated p38α (Figure 5) but do not prove that this causes prevention of activation by MKK6. The purine site compounds also bind to nonphosphorylated p38α and do not prevent activation. The Appendix includes rate equations for characterizing compounds that act by binding to the substrate (p38) and inhibit phosphorylation by MKK6. Use of these equations to calculate kinetic parameter values (Table 5) indicates that the pyrazolourea prevents phosphorylation by binding to p38α and probably not by p38α-competitive association with MKK6 (that would need to be over 1900-fold less potent when p38δ is the substrate). This compound has been compared with a quinoxaline (see Supporting Information; K_d over 10 μM for nonactivated p38α), which acts by ATP-competitive binding to MKK6.

(1) The IC_{50} of 8.2 nM for the pyrazolourea at 20 nM p38α ($\ll K_m$) can be used to estimate the value of the inhibition constant, K_{is}, if the compound acts by binding to p38 (see Table 6). The calculated $K_{is} = 6.0$ nM is in agreement with the $K_d = 4.0$ nM for nonactivated p38α.

(2) The IC_{50} of the pyrazolourea increases 23-fold from 8.2 to 190 nM when the concentration of p38α is increased 25-fold from 20 to 500 nM, whereas the IC_{50} of the
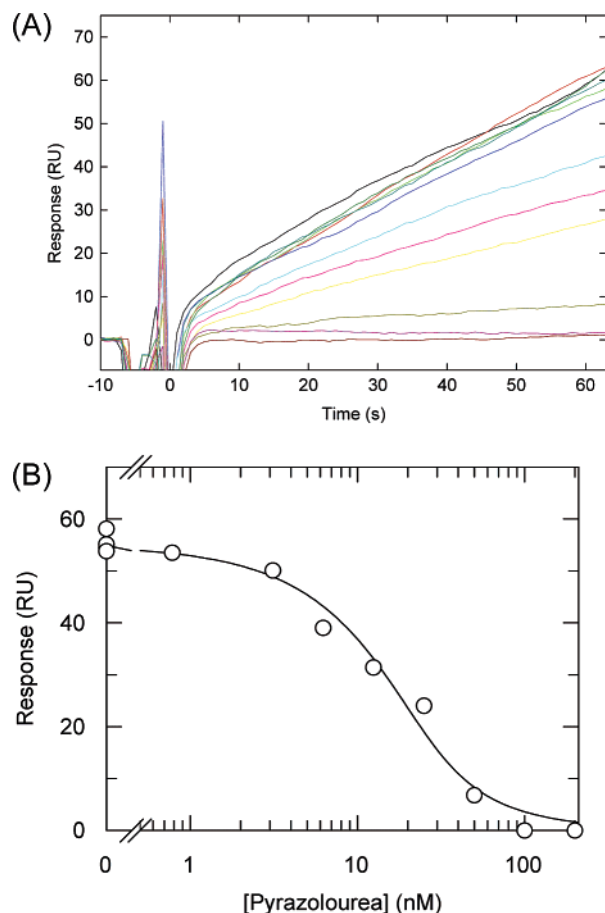
FIGURE 5: Inhibition in solution assays to estimate K_d for the pyrazolourea binding to nonactivated p38α. (A) Sensorgrams collected in the presence of various concentrations (see panel B) of the pyrazolourea are overlaid to give the same baseline and injection at $t = 0$. Details are in Experimental Procedures. (B) A plot of response at 60 s against concentration of pyrazolourea. Using eq 3, best-fit values are $K_d = 5.6$ nM (95% CIs 1.9−16 nM) and [p38α] = 22 nM (95% CIs 11−43 nM), where the expected concentration is 20 nM.

Table 5: Inhibition of MKK6-Dependent Phosphorylation of p38[a]

compound	[p38α] (nM)	[p38δ] (nM)	[ATP] (μM)	IC$_{50}$ (nM)	K_i' (nM)	[S]$_t$ (nM)
pyrazolourea	20	0	1	8.2	6.0	<22
	100	0	1	65	<30	110
	500	0	1	190	56	260
	100	0	30	56	<220	110
	0	500	1	16000	≈IC$_{50}$	ND
quinoxaline	20	0	1	7.9	≈IC$_{50}$	ND
	100	0	1	13	≈IC$_{50}$	ND
	500	0	1	23	≈IC$_{50}$	ND
	100	0	30	130	≈IC$_{50}$	ND
	0	500	1	18	≈IC$_{50}$	ND

[a] Equations A12, A20, and A23 were fitted to the data for the pyrazolourea and p38α. For the quinoxaline and each compound with p38δ, eq 1 was used. Equation 1 does not allow estimation of [S]$_t$, which is indicated as not determined (ND). Values of K_i' and [S]$_t$ are given where the upper and lower 95% CIs are within 2-fold of the best-fit values. In some cases, the experimental data do not allow precise estimation of a parameter value. If so, the value is reported as less than the upper 95% CI.

quinoxaline increases less than 3-fold from 7.9 to 23 nM. When the data for the pyrazolourea are analyzed using eqs A12, A20, and A23, which assume inhibition by binding to substrate, the estimated concentration of binding sites, [S]$_t$, is close to that of p38α.

Table 6: IC$_{50}$ Values for Prevention of Activation by Binding to Substrate[a]

	mechanism of inhibition		
total substrate concn	competitive $K_{is} \ll K_{ii}$	pure noncompetitive $K_{is} = K_{ii} = K_i$	uncompetitive $K_{is} \gg K_{ii}$
[S]$_t \ll K_m$	$K_{is} + [S]_t/2$	$K_i + [S]_t/2$	$K_{ii}K_m/[S]_t$
[S]$_t = K_m$	$2K_{is} + 2[S]_t/3$	$K_i + [S]_t/2$	$2K_{ii}$
[S]$_t \gg K_m$	$(K_{is}[S]_t/K_m) + [S]_t$	$K_i + [S]_t/2$	K_{ii}

[a] The expressions for IC$_{50}$ are derived from eq A23.

(3) ATP has a $K_m = 1.7$ μM for MKK6, and increasing the concentration from 1 to 30 μM causes a 10-fold increase in IC$_{50}$ from 13 to 130 nM for the quinoxaline and no increase for the pyrazolourea (IC$_{50}$ values of 65 and 56 nM). The elevated ATP concentration is not sufficiently high to compete for binding to nonactivated p38α, because it remains below the K_d (<10 mM; Table 2). The failure to detect ATP competing with the pyrazolourea is also due to the value of K_i' being less than 50% of the concentration of binding sites.

(4) The potency of the pyrazolourea falls by over 80-fold when the substrate is changed to p38δ (IC$_{50}$ increases from 190 to 16000 nM). Conversely, the IC$_{50}$ for the quinoxaline is almost unchanged (values of 23 and 18 nM), which is consistent with inhibition arising from binding to MKK6.

Inhibitors of p38 in Isolated Protein Assays and in Cells. Compounds can be divided into two classes according to their binding sites: purine site only (SB203580, anilinoquinazoline, Ro3201195, and pyrazoloamine) and selectivity pocket (BIRB796, MPAQ, and pyrazolourea). Binding affinities were measured by ISA. The potency for prevention of activation or inhibition of catalysis was determined as K_i'. LPS-treated THP1 cells were used to characterize effects on levels of phosphorylated p38 and production of TNFα (Table 4).

Each inhibitor exhibits only a small change in affinity when moving from nonactivated to activated p38α. Similar results have been published for SB203580 (4, 5, 40). K_d for nonactivated p38α is close to the K_i' for prevention of activation by MKK6 for the selectivity pocket compounds. Conversely, the K_i' is at least 20- to >1000-fold higher than the value of K_d for SB203580, Ro3201195, and the pyrazoloamine, which do not use the selectivity pocket. The K_i' for BIRB796 increases when MKK3 is used instead of MKK6 to phosphorylate p38α, whereas the other selectivity pocket compounds are largely unaffected. Conversely, the purine site compounds have lower K_i' values (although they are partial inhibitors) when MKK3 replaces MKK6. This may be due to effects on p38α or MKK3. The selectivity pocket compounds are less potent when p38δ replaces the α isoform as the substrate for MKK6. All of these compounds, except the anilinoquinazoline, have K_i' values for inhibition of activated p38α, which are consistent with the K_ds and the expected low degree of competition by ATP. The reasons why the anilinoquinazoline exhibits a K_i' around 10-fold lower than K_d are not known; perhaps the presence of MBP increases affinity for the enzyme.

In LPS-treated THP1 cells, SB203580 has a variable and partial effect on levels of phosphorylated p38, perhaps due to influence on processes other than MKK6-dependent phosphorylation. An IC$_{50}$ of 64 nM is seen for production of TNFα, which does not correlate with levels of phospho-

rylated p38. There are conflicting reports as to whether SB203580 does (5) or does not (4, 21, 43) prevent activation of p38 inside cells. This may reflect differences in experimental protocols and the complexity of cellular systems. Ro3201195 (purine site, $K_d = 95$ nM for nonactivated p38α) has an IC$_{50}$ for TNFα production of 200 nM and over 10 μM for prevention of activation (isolated p38α or in cells). These results suggest that inhibition of TNFα release by purine site compounds is not due to prevention of MKK6-dependent activation. Conversely, each of the selectivity pocket compounds has correlated effects on cellular levels of phosphorylated p38 and TNFα, as reported for BIRB796 (21). The IC$_{50}$ values for decreased phosphorylation in cells tend to be higher than the K_i' values in MKK6-dependent p38α phosphorylation, perhaps reflecting depletion of free compound by protein binding. The results are consistent with prevention of MKK6-dependent activation being involved in inhibition of TNFα synthesis by selectivity pocket compounds.

DISCUSSION

Binding Modes and Conformation Changes. The side chain of Phe169 may be located in a hydrophobic region of the selectivity pocket (DFG-in) or displaced to a DFG-out conformation by a suitable inhibitor, as exemplified in the complexes with the pyrazolourea and MPAQ in this study and as described elsewhere for BIRB796 (19). A DFG-in conformation usually is seen when compounds occupy only the purine site, as seen here for a pyrazoloamine and previously reported for an anilinoquinazoline and SB203580 (22, 42). The pyrazolourea does not enter the ATP site (Figures 1G and 2D), but its inhibition of activated p38α is indirectly competitive with ATP (data not shown), because the side chain of Phe169 moves into a region normally occupied by the ribose and phosphates of ATP (19). A change to DFG-out may be of further functional significance, because Phe169 is part of a conserved sequence at the beginning of the activation loop. Similar DFG-out conformations have been observed in complexes of additional kinases with inhibitors: Imatinib·ABL (44); Bay 43-9006·BRAF (45) and AAL993·KDR (46). A pattern emerges where occupation of the purine site involves formation of at least one hydrogen bond with a main-chain amide, and extension into the selectivity pocket includes a trans hydrogen-bonding arrangement with both the carboxylate of the conserved Glu and the main-chain NH of the Asp in DFG. Our structural studies of other complexes with p38α reveal that there are many positions for the side chain of Phe169, depending upon the size and nature of the groups located in, or near, the selectivity pocket. The Ro3201195 complex structure reveals a DFG-out conformation in crystals without occupying the selectivity pocket. This is unusual and may reflect the nonphysiological pH during crystallization. NMR data (Figure 4) do not detect significant conformational differences between the complexes with Ro3201195 and its pyrazoloamine analogue at either neutral or low pH, suggesting that both DFG-in and DFG-out conformers are available in solution and that crystallization stabilizes one or the other. In crystal structures for each of the current seven compounds bound to p38α, the flexibility of the docking groove results in the electron density being either poorly defined or not visible. This makes it difficult to interpret

any relationship between occupation of the selectivity pocket and structure of the docking groove. The position of the activation loop, however, clearly is affected by the DFG status (see below).

Kinetics of Binding in Different Modes. We have shown that the kinetics of complex formation for BIRB796 (Supporting Information), the pyrazolourea (Figure 3A), and MPAQ are compatible with each compound binding to nonactivated p38α that has already adopted a DFG-out conformation. This is not proof, because kinetic evidence is indirect, and the possibility remains that DFG-out is induced slowly after more rapid initial binding to form DFG-in complexes that do not accumulate. The observation of slow binding does, however, assist in understanding of structure−activity relationships for p38 inhibitors. SK&F 86002 probably binds to a DFG-in conformation and has a k_{on} of 4.3×10^7 s^{-1} M^{-1} (19), which is close to the diffusion-controlled maximum (around 10^8 s^{-1} M^{-1}) for small molecules and proteins (39). Accordingly, the free p38α and inhibitor are frequently in conformations that allow binding. Conversely, the most rapid k_{on} for a likely DFG-out compound is 15.4×10^4 s^{-1} M^{-1} for an analogue of BIRB796 (20), which is similar to the values of BIRB796 itself (Table 3 and ref 19). The slow association rate constants of selectivity pocket compounds indicate the existence of an energy barrier, which may arise from the free partners tending to be in unfavorable conformations. Ro3201195 and the pyrazoloamine each exhibit a $k_{on} > 5 \times 10^6$ s^{-1} M^{-1}, which is consistent with binding to a DFG-in conformation.

Decreases in IC$_{50}$ following preincubation indicate slow binding to activated p38α for potent selectivity pocket compounds. Bay 43-9006 exhibits similar behavior in assays of BRAF activity, with IC$_{50}$ decreasing from 0.25 μM to 4 nM after a 60 min preincubation. This compound induces a DFG-out conformation in BRAF (45). Slow binding also is seen for GW572016 binding to EGF-RTK, which again involves a conformational change, not to DFG-out, but displacement of the C-helix (47). Slow, tight-binding kinetics introduce difficulties into understanding the relationship between compound structures and biological activity. Potency in isolated enzyme assays can vary according to the duration of any preincubation, the length of the assay, and the concentration of the enzyme. It may be difficult to distinguish between compounds, which give an IC$_{50}$ equal to 50% of the concentration of binding sites. Estimation of K_d from measured on and off rates can resolve these difficulties, although these values are difficult to obtain when rates are too fast or slow.

Prevention of Activation. Phe169 is part of the conserved DFG motif at the beginning of the activation loop. Between the DFG-in and DFG-out conformations, its side chain is displaced by about 10 Å, leading to a crankshaft-like movement of the activation loop. This loop is not ordered in many crystal structures, although it is defined in the complexes of p38α with SB203580 (DFG-in) and the pyrazolourea (DFG-out). An overlay of these structures (Figure 6) reveals the possible extent of movement of the activation loop and resultant differences in the environments of the phosphoryl acceptors at Thr180 and Tyr182. DFG-out evidently results in a range of conformations, ordered or disordered, which can be accommodated in the crystals. The induced changes appear to render a productive confor-
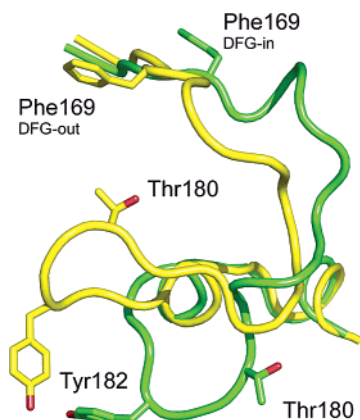
FIGURE 6: Overlay of activation loops from DFG-in and DFG-out p38α crystal structures, illustrating the possible extent of conformation change. The DFG-out conformations are linked with suboptimal rates of phosphorylation by MKK6. Main chains are overlaid for residues 165−195 in complexes with SB203580 (DFG-in, activation loop in green) and a pyrazolourea (DFG-out, activation loop in yellow).
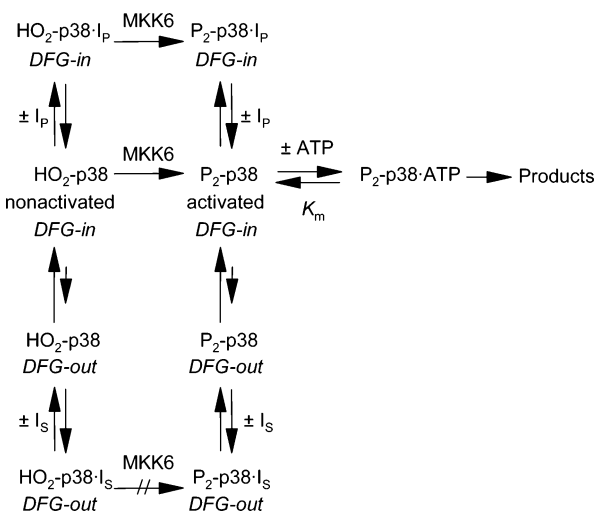

FIGURE 7: Proposed kinetic scheme for prevention of activation and inhibition of catalysis: I_P, compound binding only in the purine site; I_S, compound binding in the selectivity pocket. Weaker binding of ATP to nonactivated p38α is not shown.

mation for MKK6-dependent phosphorylation less accessible and so prevent activation.

Prevention of activation could be by a competitive mechanism (interfering with formation of the MKK6−p38α complex) or by an uncompetitive mechanism (inhibition of phosphorylation in the complex). Both of these mechanisms could occur concurrently, giving noncompetitive inhibition (see Appendix). The K_i' value for the pyrazolourea in prevention of activation assays when [p38α] ≪ K_m is close to the K_d value, indicating that inhibition is either competitive or noncompetitive (Tables 4 and 6). The K_i' increases from 6.0 nM (95% CIs 3.3−11) at 20 nM p38α to 56 nM (28−110) at 500 nM p38α, which tentatively suggests competitive inhibition (Tables 5 and 6). The observation of partial inhibition for some compounds (Table 4) indicates that phosphorylation can occur at a reduced rate when they are bound in a complex containing p38α and MKK6. Compounds differ in the extent of partial inhibition, which may correlate with induction of different distributions between a range of conformational states.

A putative kinetic scheme for the prevention of activation and inhibition of catalysis is shown in Figure 7. Free nonactivated p38α and free activated p38α are each in equilibria between DFG-in (favored) and DFG-out conformations. MKK6 can activate DFG-in conformations, regardless of whether a compound, I_P, is bound in the purine site. Some compounds, I_S, can bind in the selectivity pocket only if p38α is in a DFG-out conformation, leading to the rate of MKK6-dependent activation being reduced (to zero for a subset of I_S compounds). Following activation of p38α, there is stronger competition by ATP for binding of inhibitors to the purine site or the selectivity pocket.

This is not the first report of prevention of activation by binding to a kinase, which is a substrate for an upstream activating enzyme. PD098059 and CI-1040 bind to MAP kinase kinase 1 (MEK1) and interfere with its phosphorylation by cRAF (*48*, *49*). Analogues of these compounds bind to a complex containing nonactivated MEK and ATP, and the C-helix is displaced, probably explaining the additional mechanism of inhibition of catalysis by activated MEK (*50*).

Implications for Drug Discovery. The selectivity pocket represents an alternative to the purine site in the design of p38 inhibitors. Compounds also may extend across both sites. These multiple binding modes increase the scope for design of compounds with diversity in chemical and biological properties. Occupation of the selectivity pocket not only inhibits activated p38 but also prevents MKK6-dependent activation. This additional mode of action may have implications for biological activity in vivo. The concentrations of ADP and ATP in isolated protein assays often are much lower than the 1−2 mM levels inside cells (*51*). These metabolites are bound more weakly by p38α prior to activation, so that they compete more for inhibition of catalysis than for prevention of activation (Table 2 and refs *5* and *52*). The slow off rates for potent selectivity pocket compounds may influence pharmacokinetics (metabolism and clearance) and the duration of biological effect. BIRB796 decreases LPS-stimulated phosphorylation of p38 in human volunteers (*53*), indicating that prevention of activation occurs in vivo. The current study suggests that prevention of activation inside cells arises from binding to p38α (Table 4).

Following activation, there is less diversity in kinase 3D structure. This reflects variation in regulatory mechanisms in the nonactivated states and the evolutionary selection pressure for conservation of the catalytic site in order to facilitate similar ATP-dependent phosphotransfer reactions in the activated states (*54*, *55*). Accordingly, compounds that act by preventing kinase activation may be more selective than compounds that act only by inhibition of activated kinases (*15*, *52*).

Hit identification assays can be designed to favor compounds that use a specific site (e.g., selectivity pocket compounds prevent MKK6-dependent phosphorylation of nonactivated p38α, whereas purine site compounds only inhibit catalysis by activated p38α). There are a number of challenges in the identification and characterization of compounds that prevent activation:

(1) Phosphorylation assays need to be configured to identify compounds that act by binding to substrate. The target kinase should be dephosphorylated. For competitive or noncompetitive compounds, the assay is most sensitive

if the uninhibited rate is linear with substrate concentration ($[S]_t \ll K_m$) (see Appendix). This does bias away from uncompetitive compounds, so that $[S]_t = K_m$ may be a suitable compromise.

(2) To measure potency, $[S]_t$ should be $\ll [I]_t$. So, $[S]_t$ may be much lower than in many enzyme assays. Care is needed to avoid substrate depletion. Preincubation of substrate and inhibitor may be required for the steady-state approximation to be valid.

(3) The mechanism of active compounds must be deconvoluted to determine if they function by associating with the substrate or the upstream activating kinase. Binding studies alone are not sufficient; enzyme activity assays also are needed.

(4) Unconventional equations are required to analyze the dose−response data (see Appendix and Figure 9).

Understanding the relationship between compound structure and biological activity is key to drug design. The current study reinforces the importance of ensuring that measurements of IC_{50} are not perturbed by slow or tight binding. Even so, IC_{50} values may not correlate with affinity (e.g., purine site compounds do not prevent activation). Inhibition of catalysis may arise from binding at different sites, including the purine site, selectivity pocket, and docking groove, which follow different structure−activity relationships. Knowledge of mode of action allows classification of active compounds into subsets whose members follow the same structure−activity relationship. It is desirable to identify the target form of the enzyme (e.g., nonactivated or activated), to design a suitable assay to measure IC_{50}, to determine how to calculate the inhibition constant from the IC_{50} value, and to obtain a crystal structure of the complex between the inhibitor and the enzyme in a relevant conformation.

Summary. Compounds that enter the selectivity pocket and induce a DFG-out conformation of p38α prevent MKK6-dependent activation in addition to inhibiting catalysis by activated p38α. A one-step mechanism is adequate to explain the observed slow binding into the selectivity pocket, apparently because compounds associate directly with a DFG-out conformation, which is a minor form of free p38α. ATP binds more weakly to p38α prior to activation, so that it competes less effectively for prevention of activation than for inhibition of catalysis.

ACKNOWLEDGMENT

APPENDIX

Kinetics of Inhibition by Binding to Substrate. Compounds that act by binding to an enzyme follow conventional kinetics (eqs 1−4). Inhibition also may be due to association with free, or bound, substrate (Figure 8). Rate equations for such
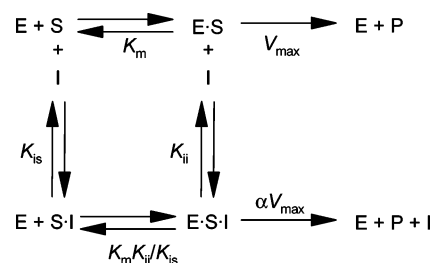

FIGURE 8: Kinetic scheme for inhibition by binding to substrate. Values of $0 < \alpha < 1$ give partial inhibition.

alternative mechanisms are derived below. An approximation to steady state is assumed, along with ATP dependence not changing with substrate concentration, $[I]_t \gg [E]_t$, and full inhibition ($\alpha = 0$ in Figure 8). K_{is} is the inhibition constant when $[S]_t \ll K_m$ and K_{ii} is that when $[S]_t \gg K_m$. As only the E·S complex may turnover to product, the rate relative to V_{max} is given by the expression

$$\frac{v}{V_{max}} = \frac{[\text{E·S}]}{[\text{E}] + [\text{E·S}] + [\text{E·S·I}]} \tag{A1}$$

where

$$K_m = [\text{E}][\text{S}]/[\text{E·S}] \tag{A2}$$

$$K_{is} = [\text{S}][\text{I}]/[\text{S·I}] \tag{A3}$$

Conservation of mass dictates that

$$[\text{S}]_t = [\text{S}] + [\text{S·I}] + [\text{E·S}] + [\text{E·S·I}] \tag{A4}$$

$$[\text{I}]_t = [\text{I}] + [\text{S·I}] + [\text{E·S·I}] \tag{A5}$$

Under the assay conditions, $[S]_t \gg [E]_t$ and $[I]_t \gg [E]_t$, so that

$$[\text{S}]_t \approx [\text{S}] + [\text{S·I}] \tag{A6}$$

$$[\text{I}]_t \approx [\text{I}] + [\text{S·I}] \tag{A7}$$

Combining eqs A3 and A6 gives

$$[\text{S}] = [\text{S}]_t/(1 + [\text{I}]/K_{is}) \tag{A8}$$

Equation A3 rearranges to

$$[\text{S·I}] = [\text{S}][\text{I}]/K_{is} \tag{A9}$$

Substitution of eqs A8 and A9 into eq A7 gives

$$[\text{I}]_t = [\text{I}]\left(1 + \frac{[\text{S}]_t}{K_{is}(1 + [\text{I}]/K_{is})}\right) \tag{A10}$$

which rearranges to

$$[\text{I}]^2 + [\text{I}](K_{is} + [\text{S}]_t - [\text{I}]_t) - [\text{I}]_t K_{is} = 0 \tag{A11}$$

This quadratic equation has only one root where $[I]$ is positive, which is

$$[\text{I}] = \{([\text{I}]_t - K_{is} - [\text{S}]_t) + \sqrt{(K_{is} + [\text{S}]_t - [\text{I}]_t)^2 + 4[\text{I}]_t K_{is}}\}/2 \tag{A12}$$
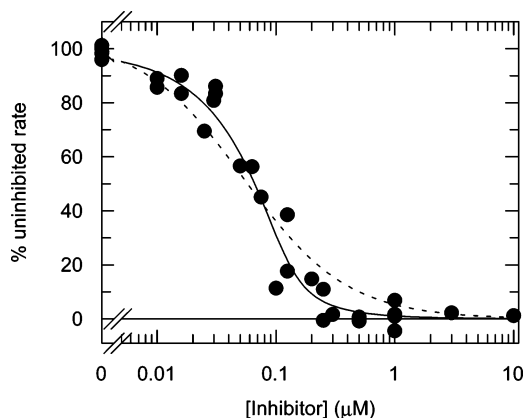
FIGURE 9: Dose−response analysis for inhibitor binding substrate. The pyrazolourea was tested in an assay for MKK6-dependent phosphorylation of p38α. Key: dashed line, best fit for eq 1 (I binds E); solid line, best fit for eqs A12 and A20 (I binds S).

Note that if $[S]_t \ll [I]_t$, then $[I] \approx [I]_t$. Or, if $[S]_t \ll K_{is} \gg [I]_t$, then $[I] \approx [I]_t$. Equation A2 rearranges to

$$[E \cdot S] = [E][S]/K_m \qquad (A13)$$

and by definition

$$K_{ii} = [E \cdot S][I]/[E \cdot S \cdot I] \qquad (A14)$$

$$\therefore [E \cdot S \cdot I] = [E \cdot S][I]/K_{ii} = [E]([S]/K_m)([I]/K_{ii}) \quad (A15)$$

so that eq A1 becomes

$$\frac{v}{V_{max}} = \frac{[S]/K_m}{1 + [S]/K_m + [S][I]/K_m K_{ii}} \qquad (A16)$$

where [S] and [I] relate to *free* concentrations, which may be lower than *total* concentrations. The value of [S] can be calculated using eq A8, so that eq A16 becomes

$$\frac{v}{V_{max}} = \frac{[S]_t}{K_m(1 + [I]/K_{is}) + [S]_t(1 + [I]/K_{ii})} \quad (A17)$$

This is identical to the conventional equation for inhibition by binding to E and E·S (*56*). It is valid for compounds that bind S *only* if $[I]_t \approx [I]$. When the rate in the presence of I is 50% of that in its absence, then [I] is equal to the apparent inhibition constant, K_i'. Substituting into eq A17 and rearranging

$$K_i' = \frac{K_{is} K_{ii}(K_m + [S]_t)}{K_m K_{ii} + [S]_t K_{is}} \qquad (A18)$$

It is possible to simplify eq A18 if separate values are not required for K_{is} and K_{ii} (Table 6). For pure noncompetitive inhibition, $K_{is} \approx K_{ii}$, so that a single K_i value may be used. Kinetics are competitive if $K_{ii} \gg K_{is}$ (K_{ii} is not required) or uncompetitive if $K_{is} \gg K_{ii}$ (K_{is} not required).

The uninhibited rate, v_0, relative to V_{max} is given by rearranging the Michaelis−Menten equation to

$$\frac{v_0}{V_{max}} = \frac{[S]_t}{K_m + [S]_t} \qquad (A19)$$

Combining eqs A17, A18, and A19

$$v = \frac{v_0}{1 + [I]/K_i'} \qquad (20)$$

Equation A20 may be used for dose−response analysis, where [I] is given by eq A12 and K_i' is given by eq A18.

Use of these equations is illustrated in Figure 9. The pyrazolourea was tested in an assay for MKK6-dependent phosphorylation of 100 nM p38α. Equation 1 (I binds E) gives an incorrect estimate of $K_i' = 53$ nM, whereas eqs A12 and A20 (I binds S) give the correct $K_i' = 10$ nM and an accurate measure of the concentration of binding sites, $[S]_t = 110$ nM. The residual differences between the best-fit lines and the experimental data are more systematic for eq 1, indicating a poorer quality of fit (*35*).

(A) IC$_{50}$ Values for Compounds That Inhibit by Binding to Substrate. These values reflect free and bound inhibitor, so that

$$IC_{50} = [I]_t = K_i' + [I]_b \qquad (A21)$$

where K_i' is free I and $[I]_b$ is bound I, which $\approx [S \cdot I]$, giving

$$IC_{50} = K_i' + [S][I]/K_{is} \qquad (A22)$$

$[I] = K_i'$ and [S] is given by eq A8, so that

$$IC_{50} = K_i' + \frac{[S]_t K_i'}{K_{is} + K_i'} \qquad (A23)$$

Equation A23 can be modified to give the IC$_{50}$ for different mechanisms of inhibition at various concentrations of substrate (Table 6). This analysis indicates that it may be difficult to distinguish between competitive and pure noncompetitive compounds, especially if there is uncertainty in the magnitude of the concentration of binding sites, $[S]_t$. Rate equations previously have been derived for some of these systems (*57−59*), although the current format with IC$_{50}$ values is aimed to be particularly suitable for drug discovery.

(B) Kinetic Equivalence. The relationships for I binds S generate several examples of kinetic equivalence, where different physical mechanisms lead to the same rate equation (*39*). Equation A18 was reported for systems where I binds E by Cheng and Prusoff (*37*). The two different models for tight-binding inhibition ($[I]_f < [I]_t$) for I binds S and I binds E follow similar rate equations. This can be observed by fitting eq 3 (I binds E) or eq A12 with eq A20 (I binds S) to the same data set. The two models give the same values for K_i', and the estimated values for $[E]_t$ from eq 3 are the same as those for $[S]_t$ from eq A12. A further example of kinetic equivalence arises for uncompetitive compounds: those binding S when $[S] \gg K_m$ give the same IC$_{50}$ values (Table 6) as uncompetitive compounds that bind E when $[S] \gg K_m$.

SUPPORTING INFORMATION AVAILABLE

Further descriptions and evaluations for the following experimental procedures: expression, labeling, and purification of human recombinant p38α; compounds used as molecular tools; inhibition in solution assays to measure binding affinity; binding kinetics for BIRB796. This material

is available free of charge via the Internet at http:// pubs.acs.org.

REFERENCES

1. Lee, J. C., Kassis, S., Kumar, S., Badger, A., and Adams, J. L. (1999) p38 mitogen-activated protein kinase inhibitors—mechanisms and therapeutic potentials, *Pharmacol. Ther. 82*, 389−397.

2. Kumar, S., Boehm, J., and Lee, J. C. (2003) p38 MAP kinases: key signalling molecules as therapeutic targets for inflammatory diseases, *Nat. Rev. Drug Discov. 2*, 717−726.

3. Pargellis, C., and Regan, J. (2003) Inhibitors of p38-mitogen-activated protein kinase for the treatment of rheumatoid arthritis, *Curr. Opin. Invest. Drugs 4*, 566−571.

4. Young, P. R., McLaughlin, M. M., Kumar, S., Kassis, S., Doyle, M. L., McNulty, D., Gallagher, T. F., Fisher, S., McDonnell, P. C., Carr, S. A., Huddleston, M. J., Seibel, G., Porter, T. G., Livi, G. P., Adams, J. L., and Lee, J. C. (1997) Pyridinyl imidazole inhibitors of p38 mitogen-activated protein kinase bind in the ATP site, *J. Biol. Chem. 272*, 12116−12121.

5. Frantz, B., Klatt, T., Pang, M., Parsons, J., Rolando, A., Williams, H., Tocci, M. J., O'Keefe, S. J., and O'Neill, E. A. (1998) The activation state of p38 mitogen-activated protein kinase determines the efficiency of ATP competition for pyridinylimidazole inhibitor binding, *Biochemistry 37*, 13846−13853.

6. Raingeaud, J., Whitmarsh, A. J., Barrett, T., Derijaard, B., and Davis, R. J. (1996) MKK3- and MKK6-gene regulated expression is mediated by the p38 mitogen-activated protein kinase signal transduction pathway, *Mol. Cell. Biol. 16*, 1247−1255.

7. Brancho, D., Tanak, M., Jaeschke, A., Ventura, J. J., Kelkar, N., Tanaka, Y., Kyuuma, M., Takeshita, T., Flavell, R. A., and Davis, R. J. (2003) Mechanism of p38 MAP kinase activation *in vivo*, *Genes Dev. 17*, 1969−1978.

8. Ge, B., Gram, H., Padova, F., Huang, B., New, L., Ulvetich, R. J., Luo, Y., and Han, J. (2002) MAPKK-independent activation of p38α mediated by TAB1-dependent autophosphorylation of p38α, *Science 295*, 1291−1294.

9. Wang, Z., Harkins, P. C., Ulevitch, R. J., Han, J., Cobb, M. H., and Goldsmith, E. J. (1997) The structure of mitogen-activated protein kinase p38 at 2.1 Å resolution, *Proc. Natl. Acad. Sci. U.S.A. 94*, 2327−2332.

10. Bellon, S., Fitzgibbon, M. J., Fox, T., Hsiao, H.-M., and Wilson, K. P. (1999) The structure of phosphorylated p38γ is monomeric and reveals a conserved activation-loop conformation, *Structure 7*, 1057−1065.

11. Johnson, L. N., Noble, M. E. M., and Owen, D. J. (1996) Active and inactive protein kinases: Structural basis for regulation, *Cell 85*, 149−158.

12. Chang, C.-I., Xu, B.-e., Akella, R., Cobb, M. H., and Goldsmith, E. J. (2002) Crystal structures of MAP kinase p38 complexed to the docking sites on its nuclear substrate MEF2A and activator MKK3b, *Mol. Cell 9*, 1241−1249.

13. Adams, J. A. (2003) Activation loop phosphorylation and catalysis in protein kinases. Is there functional evidence for the autoinhibitor model?, *Biochemistry 42*, 601−607.

14. Cherry, M., and Williams, D. H. (2004) Recent kinase and kinase inhibitor X-ray structures: Mechanisms of inhibition and selectivity insights, *Curr. Med. Chem. 11*, 663−673.

15. Cohen, P. (2002) Protein kinases—the major drug targets of the twenty-first century?, *Nat. Rev. Drug Discov. 1*, 309−315.

16. Lisnock, J. M., Tebben, A., Frantz, B., O'Neill, E. A., Croft, G., O'Keefe, S. J., Li, B., Hacker, C., de Laszlo, S., Smith, A., Libby, B., Liverton, N., Hermes, J., and LoGrasso, P. (1998) Molecular basis for p38 protein kinase inhibitor specificity, *Biochemistry 37*, 16573−16581.

17. Cumming, J. G., McKenzie, C. L., Bowden, S. G., Campbell, D., Masters, D. J., Breed, J., and Jewsbury, P. J. (2004) Novel, potent and selective anilinoquinazoline and anilinopyrimidine inhibitors of p38 MAP kinase, *Bioorg. Med. Chem. Lett. 14*, 5389−5394.

18. Dumas, J., Hatoum-Mokdad, H., Sibley, R., Riedl, B., Scott, W. J., Monahan, M. K., Lowinger, T. B., Brennan, C., Natero, R., Turner, T., Johnson, J. S., Schoenleber, R., Bhargava, A., Wilhelm, S. M., Housely, T. J., Ranges, G. E., and Shrikhande, A. (2000) 1-phenyl-5-pyrazolyl ureas: Potent and selective p38 kinase inhibitors, *Bioorg. Med. Chem. Lett. 10*, 2051−2054.

19. Pargellis, C., Tong, L., Churchill, L., Cirillo, P. F., Gilmore, T., Graham, A. G., Grob, P. M., Hickey, E. R., Moss, N., Pav, S., and Regan, J. (2002) Inhibition of p38 MAP kinase by utilizing a novel allosteric site, *Nat. Struct. Biol. 9*, 268−272.

20. Regan, J., Pargellis, C. A., Cirillo, P. F., Gilmore, T., Hickey, E. R., Peet, G. W., Proto, A., Swinamer, A., and Moss, N. (2003) The kinetics of binding to p38 MAP kinase by analogues of BIRB 796, *Bioorg. Med. Chem. Lett. 13*, 3101−3104.

21. Kuma, Y., Sabio, G., Bain, J., Shapiro, N., Márquez, R., and Cuenda, A. (2005) BIRB0796 inhibits all p38 MAPK isoforms *in vitro* and *in vivo*, *J. Biol. Chem. 280*, 19472−19479.

22. Shewchuk, L., Hassell, A., Wisely, B., Rocque, W., Holmes, W., Veal, J., and Kyper, L. F. (2000) Binding mode of the 4-anilinoquinazoline class of protein kinase inhibitor: X-ray crystallographic studies of 4-anilinoquinazolines bound to cyclin-dependent kinase 2 and p38 kinase, *J. Med. Chem. 43*, 133−138.

23. Gallagher, T. F., Seibel, G. L., Kassis, S., Laydon, J. T., Blumenthal, M. J., Lee, J. C., Lee, D., Boehm, J. C., Fier-Thompson, S. M., Abt, J. W., Soreson, M. E., Smietana, J. M., Hall, R. F., Garigipati, R. S., Bender, P. E., Erhard, K. F., Krog, A. J., Hoffmann, G. A., Sheldrake, P. L., McDonnell, P. C., Kumar, S., Young, P. R., and Adams, J. L. (1997) Regulation of stress-induced cytokine production by pyridinylimidazoles; Inhibition of CSBP kinase, *Bioorg. Med. Chem. 5*, 49−64.

24. Crawley, G. C., McKerrecher, D., Poyser, J. P., Hennequin, L. F., Ple, P., and Lambert, C. M.-P. (2001) Quinazoline derivatives, International Patent WO 01/04102.

25. Labadie, S. S., Rotstein, D. M., Sjogren, E. B., and Talamas, F. X. (1999) Preparation of 5-aminopyrazole derivatives as p38 MAP kinase inhibitors, International Patent WO 99/57101.

26. Leslie, A. G. W. (1992) Recent changes to the MOSFLM package for processing film and image plate data, *Joint CCP4 + ESF-EAMCB Newsletter on Protein Crystallography*, No. 26.

27. Collaborative Computational Project, Number 4 (1994) The CCP4 suite: Programs for protein crystallography, *Acta Crystallogr. D50*, 760−763.

28. Murshudov, G. N., Vagin, A. A., and Dodson, E. J. (1997) Refinement of Macromolecular structures by the maximum-likelihood method, *Acta Crystallogr. D53*, 240−255.

29. Tugarinov, V., Muhandiram, R., Ayed, A., and Kay, L. E. (2002) Four-dimensional NMR spectroscopy of a 723-residue protein: Chemical shift assignments and secondary structure of malate synthase G, *J. Am. Chem. Soc. 124*, 10025−10035.

30. Loria, J. P., Rance, M., and Palmer, A. G., III (1999) Transverse-relaxation-optimized (TROSY) gradient-enhanced triple-resonance NMR spectroscopy, *J. Magn. Reson. 141*, 180−184.

31. Delaglio, F., Grzesiek, S., Vuister, G. W., Zhu, G., Pfeifer, J., and Bax, A. (1995) NMRPipe: A multidimensional spectral processing system based on UNIX pipes, *J. Biomol. NMR 6*, 277−293.

32. Johnson, B. A., and Blevins, R. A. (1994) NMRView: A computer program for the visualization and analysis of NMR data, *J. Biomol. NMR 4*, 603−614.

33. Karlsson, R. (1994) Real-time competitive analysis of interactions between low-molecular-weight ligands in solution and surface-immobilized receptors, *Anal. Biochem. 221*, 142−151.

34. Leatherbarrow, R. J. (1996) GraFit (Version 3.09b), Erithacus Software, Staines, U.K.

35. Mannervik, B. (1982) Regression analysis, experimental error, and statistical criteria in the design and analysis of experiments for discrimination between rival kinetic models, *Methods Enzymol. 87*, 370−390.

36. Christopoulos, A. (1998) Assessing the distribution of parameters in models of ligand−receptor interaction: to log or not to log, *Trends Pharmacol. Sci. 19*, 351−357.

37. Cheng, Y.-C., and Prusoff, W. H. (1973) Relationship between the inhibition constant (K_I) and the concentration of inhibitor which causes 50 percent inhibition (I_{50}) of an enzymatic reaction, *Biochem. Pharmacol. 22*, 3099−3108.

38. Morrison, J. F., and Walsh, C. T. (1988) The behaviour and significance of slow-binding enzyme inhibitors, *Adv. Enzymol. 61*, 201−301.

39. Fersht, A. R. (1998) *Structure and mechanism in protein science*, W. H. Freeman, New York.

40. LoGrasso, P. V., Frantz, B., Rolando, A. M., O'Keefe, S. J., Hermes, J. D., and O'Neill, E. A. (1997) Kinetic mechanism for p38 MAP kinase, *Biochemistry 36*, 10422−10427.

41. Chen, G., Porter, M. D., Bristol, J. R., Fitzgibbon, M. J., and Pazhanisamy, S. (2000) Kinetic mechanism of the p38α MAP kinase: Phosphoryl transfer to synthetic peptides, *Biochemistry 39*, 2079−2087.

42. Wang, Z., Canagarajah, B. J., Boehm, J. C., Kassisà, S., Cobb, M. H., Young, P. R., Abdel-Meguid, S., Adams, J. L., and Goldsmith, E. J. (1998) Structural basis of inhibitor selectivity in MAP kinases, *Structure 6*, 1117−1128.

43. Kumar, S., Jiang, M. S., Adams, J. L., and Lee, J. C. (1999) Pyridinylimidazole compound SB203580 inhibits the activity but not the activation of p38 mitogen-activated protein kinase, *Biochem. Biophys. Res. Commun. 263*, 825−831.

44. Schindler, T., Bornmann, W., Pellicena, P., Miller, W. T., Clarkson, B., and Kuriyan, J. (2000) Structural mechanism for STI-571 inhibition of Abelson tyrosine kinase, *Science 289*, 1938−1942.

45. Wan, P. T. C., Bargett, M. J., Roe, S. M., Lee, S., Niculescu-Duvaz, D., Good, V. M., Cancer Genome Project, Jones, C. M., Marshall, C. J., Springer, C. J., and Marais, R. (2004) Mechanism of activation of the RAF-ERK singaling pathway by oncogenic mutations of B-RAF, *Cell 116*, 855−867.

46. Manley, P. W., Bold, G., Brüggen, J., Fendrich, G., Furet, P., Mestan, J., Schnell, C., Stolz, B., Meyer, T., Meyhack, B., Stark, W., Strauss, A., and Wood, J. (2004) Advances in the structural biology, design and clinical development of VEGF-R kinase inhibitors for the treatment of angiogenesis, *Biochim. Biophys. Acta 1697*, 17−27.

47. Wood, E. R., Truesdale, A. T., McDonald, O. B., Yuan, D., Hassell, A., Dickerson, S. H., Ellis, B., Pennisi, C., Horne, E., Lackey, K., Alligood, K. J., Rusnak, D. W., Gilmer, T. M., and Shewchuk, L. (2004) A unique structure for epidermal growth factor receptor bound to GW572016 (lapatinib): Relationship among protein conformation, inhibitor off-rate, and receptor activity in tumour cells, *Cancer Res. 64*, 6652−6659.

48. Alessi, D. R., Cuenda, A., Cohen, P., Dudley, D. T., and Saltiel, A. R. (1995) PD 098059 is a specific inhibitor of mitogen-activated protein kinase kinase *in vitro* and *in vivo*, *J. Biol. Chem. 270*, 27489−27494.

49. Davies, S. P., Reddy, H., Caivano, M., and Cohen, P. (2000) Specificity and mechanism of action of some commonly used protein kinase inhibitors, *Biochem. J. 351*, 95−105.

50. Ohren, J. F., Chen, H., Pavlovsky, A., Whitehead, C., Zhang, E., Kuffa, P., Yan, C., McConnell, P., Spessard, C., Banotai, C., Mueller, W. T., Delaney, A., Omer, C., Sebolt-Leopold, J., Dudley, D. T., Leung, I. K., Flamme, C., Warmus, J., Kaufman, M., Barrett, S., Tecle, H., and Hasemann, C. A. (2004) Structures of human MAP kinase kinase 1 (MEK1) and MEK2 describe novel noncompetitive kinase inhibition, *Nat. Struct. Mol. Biol. 11*, 1192−1197.

51. Greenbaum, A. L., Gumaa, K. A., and McLean, P. (1971) The distribution of hepatic metabolites and the control of pathways of carbohydrate metabolism in animals of different dietary and hormonal status, *Arch. Biochem. Biophys. 143*, 617−663.

52. Knight, Z. A., and Shokat, K. M. (2005) Features of selective kinase inhibitors, *Chem. Biol. 12*, 621−637.

53. Branger, J., van den Blink, B., Weijer, S., Madwed, J., Bos, C. L., Gupta, A., Yong, C.-L., Polmar, S. H., Olszyna, D. P., Hack, C. E., van Deventer, S. J. H., Peppelenbosch, M. P., and van der Poll, T. (2002) Anti-inflammatory effects of a p38 mitogen-activated protein kinase inhibitor during endotoxemia, *J. Immunol. 168*, 4070−4077.

54. Hubbard, S. R., and Till, J. H. (2000) Protein tyrosine kinase structure and function, *Annu. Rev. Biochem. 69*, 373−398.

55. Huse, M., and Kuriyan, J. (2002) The conformational plasticity of protein kinases, *Cell 109*, 275−282.

56. Cleland, W. W. (1963) The kinetics of enzyme-catalyzed reactions with two or more substrates or products. II. Inhibition: nomenclature and theory, *Biochim. Biophys. Acta 67*, 173−187.

57. Segel, I. H. (1975) in *Enzyme Kinetics*, pp 203−208, Wiley, New York.

58. Morrison, J. F., and Cleland, W. W. (1980) A kinetic method for determining dissociation constants for metal complexes of adenosine 5′-triphosphate and adenosine 5′-disphosphate, *Biochemistry 19*, 3127−3131.

59. Morrison, J. F., and Cleland, W. W. (1983) Lanthanide-adenosine 5′-triphosphate complexes: Determination of their dissociation constants and mechanism of action as inhibitors of yeast hexokinase, *Biochemistry 22*, 5507−5513.